Measurement microscale vibration information with living biological probes

Chen, Ziqing; Jiang, Chunlei ; Yan, Bing; Yue, Liyang; Chen, Peng

Optics Communications

DOI:
10.1016/j.optcom.2021.127823

Published: 15/04/2022

Peer reviewed version

Measurement microscale vibration information with living biological probes

Ziqing Chen[a], Chunlei Jiang[a], Bing Yan[b,c], Liyang Yue[c], Peng Chen[a]

[a] College of Electrical and Information Engineering, Northeast Petroleum University, Daqing 163318, China
[b] Center of Optics Health, Suzhou Institute of Biomedical Engineering and Technology, Chinese Academy of Sciences, No. 88 Keling Street, Suzhou Jiangsu, 215163, China
[c] School of Computer Science and Electronic Engineering, Bangor University, Dean Street, Bangor, Gwynedd, LL57 1UT, UK

Abstract
We report on the first demonstration of a living biological probe that is utilized to measure microscale vibration information. The microsphere-based living biological probes were precisely manipulated through optical fiber tweezers technology, enabling to transmission and focus of the emitted light on the surface of the vibrating microstructure and then combining it with laser self-mixing interference to obtain the microscale vibration information. Experiments show that the living probes can successfully detect the microscale vibration information of microstructure, and the relationship between the interference fringe number of the self-mixing signal and the peak-to-peak amplitude of the vibration of the microstructure was analyzed. The presented living probes may expand the application of optical fiber probes for detecting microscale vibration information in the biological field.

Keywords
Laser self-mixing interference; Biological microsphere superlens; Optical fiber tweezers; Microscale displacement measurement

1. Introduction

Self-mixing interference (SMI) is attractive for optical measurements in many fields, such as structural analysis [1], micro-damping vibration [2], [3], [4], motor runout [5], [6], [7], and medical diagnosis [8], [9], [10], [11], due to its inherent simplicity, compactness, and self-alignment [12]. Microscale vibration information can be easily obtained by using the SMI effect. In recent years, microscale vibration measurements of certain organisms in the solution environment have been an interesting study in the field of microbiology [11], [13], [14]. Exploring a new sensing measurement method applicable to the biological environment is important.

Fiber probes are processed so that the small tip can be used as a convenient probe into narrow biological sample chambers for the detection of microstructures. However, the current processing of fiber probes is flame-burned and stretched, which does not guarantee the regular shape of the processed fiber ends. Some of the proposed probe structures are composed of high refractive index inorganic materials, such as precious metals and semiconductors [15], which will mechanically damage samples, particularly biological cells and tissues, during manipulation and measurement [15], [16]. For example, near-field optical scanning probes coated with precious metal nanofilms or attached with semiconductor nanowires or nanocavities will easily pierce cell membranes under measurement and manipulation, and local heating is caused by light absorption from high-refractive-index materials will cause undesired photothermal damage to biological samples [17], [18]. Therefore, a measurement tool suitable for the detection of microstructural displacements in biological environments in combination with optical interferometry is lacking. This condition calls for a new sensing method incorporating the SMI principle to provide the possibility of microscale detection in biological environments. Focusing on the surface of the object to be measured is difficult due to the measurement of light diffuses in an aqueous environment, which requires small particles that can act as lenses to collect light. However, the current microspheres are commonly formed by artificially inorganic materials, such as silicon dioxide (SiO2),

titanium dioxide (TiO2), and barium titanate ($BaTiO_3$). They endure relatively low biocompatibility when interacting with biosamples in detection or sensing applications. Local heating induced by the optical absorption of the high-index materials will cause undesired photothermal damage to biospecimens [18]. Therefore, a biocompatible, harmless, and non-invasive focusing lens is needed. Biological materials, such as yeast cells [19], red blood cells [20], and spider silks [21] are found to have the ability to focus light into a limited area. They are used as biomicrolens in optical imaging. The biological materials avoid damage from artificial inorganic materials and are naturally abundant biomaterials and are fully compatible with biological systems, stimulating us to use living cells as optical devices in measurement. A mature method is required for controlling biological cells to become part of the sensor stably. Optical fiber tweezers(OFTs) have become an important tool for research in the field of bio-optics. This technology is maturely applied to the grasping and manipulation of small organisms. It plays an important role in medical diagnosis [22], biosensing [23], [24], cell exploration [19], molecular tracking [25], and other fields. Biological cells can be firmly captured at the tip of the fiber by using fiber optic tweezers.

In this study, we use natural biological cells as biological microsphere superlens(BMS), and a living probe is utilized as a method for measuring microscale displacement in a living biological cell environment. A commercial multi-mode fiber is stretched and processed, and the yeast cells are stably captured constructively at the fiber ends by using optical tweezer techniques. The yeast cells converge the detection light into a dense region to utilize the detection light on the microstructure while enhancing the reflected light from the surface of the microstructure and returning the reflected light to the laser cavity to produce SMI phenomena. We use multiple Hilbert program to retrieve the displacement of the microstructure. The proposed live probe can realize the measurement of a vibrational range larger than the half-wavelength of the LD used in the system and smaller than the length of the probe light aggregation spot. We validate the performance of the proposed live probe by measuring the displacement of the fabricated microstructure. We provide an outlook on the future application of the active probe to living organisms.

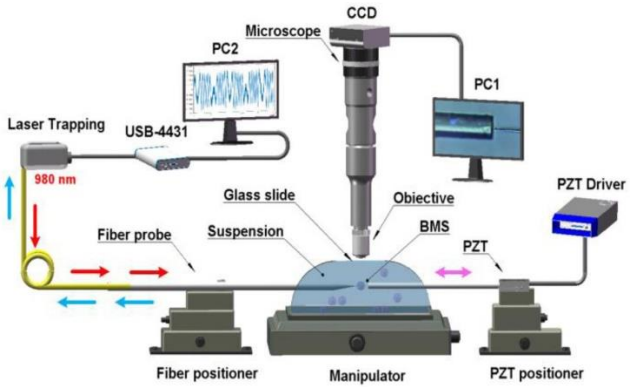

Fig. 1. Experimental setup schematic diagram of the sensor based on BMS for vibration measurement of microstructure in a liquid environment. The red and blue arrows indicate the propagation of the input laser beam (980 nm), backscattering signal (980 nm), respectively. The pink arrow indicates the vibration direction of the microstructure.

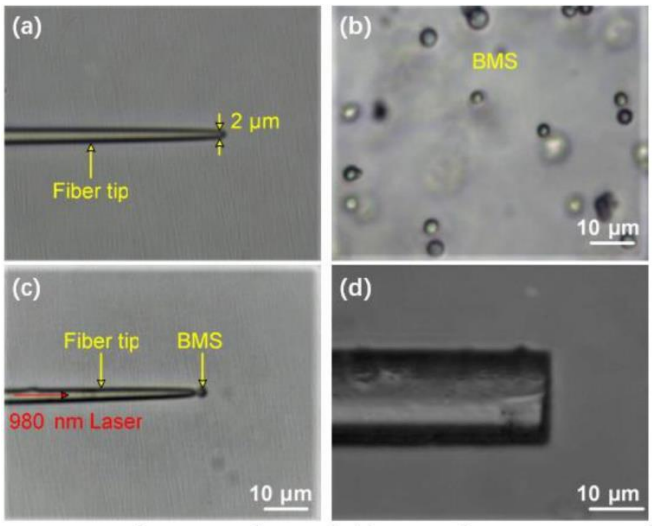

Fig. 2. Images of experimental materials. (a) An optical microscope image of a tapered fiber with a tapered tip diameter of 2 μm (b) The optical microscope image of the BMS with an average diameter of 2 μm. (c) The optical image demonstrating a BMS is trapped at the tip of an optical fiber probe. (d) The optical image demonstrates a segment of a flat tip optical fiber with diameter of 18 μm.

2. Experimental setup

Fig. 1 shows a schematic of the experimental structure. The experiment is performed under an optical microscope equipped with a charge-coupled device (CCD) camera and an objective lens (40×, NA 0.65). The sample chamber and the fiber used for capture are fixed to a manipulator and a fiber positioner, respectively. The fiber stretched into microstructure is used as a vibrating object and fixed under closed-loop control on a PZT (P753.1CD, PI) with a resolution of 0.05 nm. The PZT is fixed to a PZT positioner.

A volume of yeast cell suspension is first extracted and placed in an aqueous solution. The cells are approximately 2 μm in diameter and have a refractive index of n_b = 1.40 [19]. Immature yeast cells are chosen as BMS to facilitate the transmission of light emitted to the surface of the measured object because they have micron size, spherical shape, smooth surface, relatively high refractive index contrast, and they are harmless to human health. A syringe is used to inject the cell suspension into the sample chamber. The sample chamber is uniformly filled with the BMS solution. A fiber optic positioner is used to insert a tapered fiber into the BMS solution that can be used to capture the cells, guide the light, and collect the light signal. A 980 nm laser with an optical power of 30 mW is emitted into the optical fiber. The 980 nm laser is chosen because the light absorption and scattering of biological samples are greatly reduced in the near-infrared region (approximately 980) and light at this wavelength is weakly absorbed by biological material. This wavelength of light has a greater penetration depth and less light damage than ultraviolet and visible light excitation [26]. This condition ensures that the BMS is not damaged and that the light is better focused to measure the microstructure of the surface. The BMS can be stably captured at the tip of the tapered fiber by using optical gradient force and by moving the tapered fiber precisely close to the BMS. Benefitting from the spherical shape of the yeast cells, the captured laser beam can be focused into a convergent region. The microstructure fiber is inserted into the sample chamber, and the microorganism is simulated by using the PZT positioner. The fiber probe with BMS is aligned vertically with the surface of the microstructure, and the emitted light is ensured to be directed at the target surface by adjusting the manipulator, fiber positioner, and PZT positioner.

The front end of the sensor is positioned 2 μm from the surface of the object to be measured. The operation and measurement of the sample chamber can be viewed via the CCD and displayed on PC1 (Personal Computer). The PZT is activated to simulate the vibration of the source. The reflected light is detected by the built-in laser PD. Subsequently, a voltage signal is generated by a data acquisition module (USB-4431, NI) and processed to PC2. In this experiment, all devices are placed on an optically isolated platform (PTR52509, Thorlabs) to avoid the effects of environmental vibrations. Fig. 2(a)

shows the profile of a fiber optic probe widely used to capture biological cells. Compared with conventional optical tweezers, holographic optical tweezers and surface plasmon-based optical tweezers, OFTs possess exceptional advantages in the manipulation flexibility due to the simple structure with only optical fibers. The fiber optic probe is relatively easier to capture and manipulate cells. The fiber can be inserted into thick samples and turbid media, greatly increases the sample applicability. OFTs make optical manipulation a low-cost technique due to the easy fabrication procedures. They are a versatile candidate for optical trapping and manipulation of cells. In this work, OFTs as a tool combined with yeast cells are easy to form probe sensors for displacement measurements of microscale.

Parabolic fiber probes are prepared through a flame heating technique by using commercial multi-mode fiber probes (connector method: FC/PC, cladding diameter: 125 μm). The fibers are stripped of their buffer and polymer sheath by using a fiber stripper to obtain a bare fiber with a length of 2 cm and a diameter of 50 μm. A quartz microtube is wrapped around the fiber to hold the fiber probe in place prior to heating. The bare fiber is heated by the outer flame of an alcohol lamp for approximately 40 s. The bare fiber is stretched at a rate of 3 mm^{s1}, causing it to become progressively thinner. (The diameter of the tapered area is 10 μm). The stretching speed is increased to 10 mm^{s1} until the fiber is broken off with a parabolic tip. A size distribution of a natural BMS of size 2–3 μm is shown in Fig. 2(b). After switching on the laser, the fiber probe reaches the sample chamber. The yeast cells are stably caught by the physics of light acting on the particles, and the particles do not fall off as the fiber moves. The resultant BMS-based stable fiber-optic sensing device is shown in Fig. 2(c). Fig. 2(d) demonstrates a section of flat-tipped fiber manufactured by pulling a commercial fiber with a head face diameter of approximately 18 μm to simulate a microorganism.

Fig. 3(a)–(f) shows the manipulation of the 2D movement of a biological cell with a fiber probe to demonstrate manipulation flexibility.

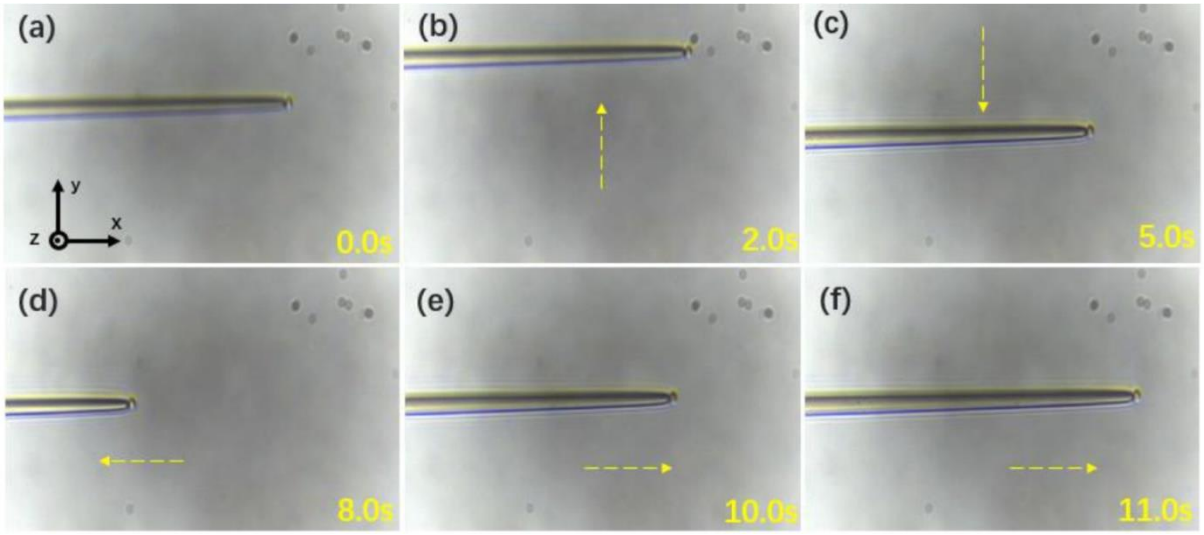

Fig. 3. (a)–(f) The process of manipulating biological cells to move 2D with fiber probe.

3. Theoretical analysis

The elementary theories of the SMI effect can be interpreted by two Fabry–Perot cavities [27], [28], [29], [30]. As expressed in Fig. 4, in which and are the amplitude reflectivity of laser diode (LD) facets, is the amplitude reflectivity of the external object, denotes the length of the internal cavity, is the length of the external cavity. The SMI signal is monitored by a photodiode (PD), which is encapsulated in the LD. SMI occurs when part of the output light is reflected or scattered into the laser cavity by the vibrating target. Eliding the multiple reflections of the external cavity, the main relationship between the SMI optical output power and the phase can be presented as follows [27], [30], [31]

$$PF = P0[1 + m\cos(\varphi F\ (t))], \quad (1)$$

where is the laser output power without optical feedback is the power with optical feedback and represents the modulation coefficient of SMI [27]. The round-trip phase change can be written as follows [27]

$$\varphi 0(t) = \varphi F\ (t) + C\ \sin[\varphi F\ (t) + \arctan\ \alpha], \quad (2)$$

where C is the feedback level parameter that depends on the amount of light reentered into the laser cavity [27]. represents the external round-trip phase without optical feedback and is the phase with optical feedback is the line-width enhancement factor. and can be written as follows

$$\varphi 0(t) = 4\pi L(\mathrm{t})/\lambda_0, \quad (3)$$

$$\varphi F\ (t) = 4\pi L(\mathrm{t})/\lambda_F. \quad (4)$$

Under weak feedback mechanism [32], it is known that, , is the wavelength without optical feedback. The length change of the external cavity can be written as follows

$$L(t) = \varphi F\ (t)\ \lambda 0/4\pi. \quad (5)$$

The tapered shape makes the capture beam highly concentrated at the tip of the optical fiber and forms a stable light capture potential. The yeast cells can be captured and trapped at the tip of the fiber by the optical gradient force and by moving the tapered fiber precisely close to the yeast cells. The captured laser beam can be focused on a small area. A theoretical model is established by using COMSOL software to study the capture stability of OFTs. The simulated environment is in aqueous solution. The wavelength of the incident light is 980 nm, and the power is 30 mW. Fig. 5(a) shows the energy density distribution of the output laser beam of the bare tapered fiber. The output laser beam is focused at the tip of the fiber. When a 2 μm yeast cell (refractive index 1.40) is captured at the tip of the fiber, a tightly focused beam is generated (Fig. 5(b)), the aggregated spot length of the transmitted light through the BMS is approximately 6 μm. This condition is due to the interference between the field scattered by the yeast cell and the large angular component of the incident Gaussian beam through the cell. The waveform of the SMI signal is related to the smoothness and focusing performance of the detector surface. The stretched fiber tip cannot guarantee the smoothness of the fiber tip and cannot play the role of focusing. The detection light shines through the non-smooth surface in the form of divergence to the measured object and returns the object motion information to the laser cavity through the nonsmooth surface in the form of divergence, thereby causing some interference effects on the obtained signal in the experiment. On the contrary, the yeast cell, as a natural lens, has a smooth surface as well as focusing characteristics, and the captured laser beam can be focused to a smaller area. When the detector surface is smooth and the detection light is focused on the central dense area, the smooth detection surface reduces the interference to the mixing signal, and the focused detection light can be focused to the surface of the object under test. In accordance with the light reflection principle, the feedback light carrying the object vibration information is returned to the laser cavity in a concentrated form. The interference of the measurement process is reduced.

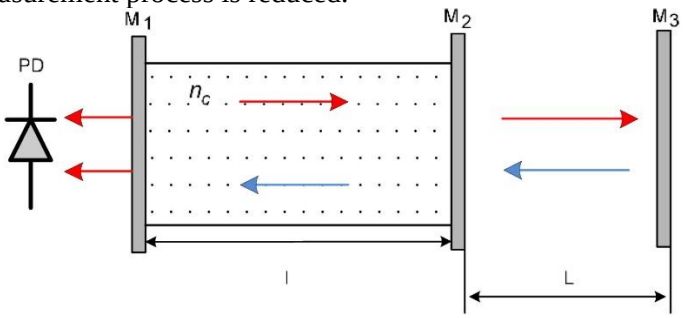

Fig. 4. Theoretical model of SMI.

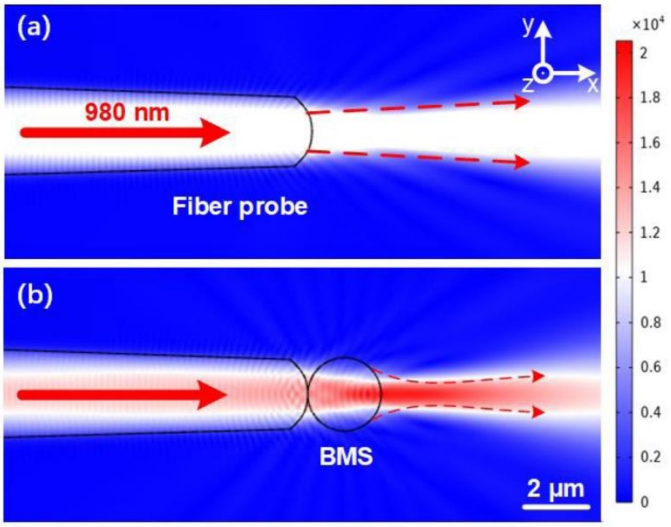

Fig. 5. Numerical simulations and calculations is in aqueous solution environment. (a) Energy distribution of the output of a bare tapered fiber in the x–y plane. (b) The tip of the tapered fiber captures a spherical yeast cell that focuses the 980 nm laser beam into an area.

4. Experimental results

As shown in Fig. 6(a), the waveform is the SMI signal collected in microscale vibration of a microstructure with a vibration frequency of 5 Hz and a peak-to-peak amplitude of 3 . In this experiment, we used bare fiber without yeast cells to measure a microstructure at the same vibration parameters and measurement distances as a comparative test. The measured SMI signal is shown in Fig. 6(b). Compared with the signals from the two experimental groups, the signal streak measured by the BMS fiber optic probe is clearer, and the displacement information of the measured object is more intuitive under the smooth surface characteristics of yeast cells and the focusing effect on light. To determine the stability of the device, we varied the vibration amplitude of the object. We conducted experiments at the same vibration frequency (5 Hz) and selected amplitudes between 1.0 μm to 4.0 μm with a step size of 1.0 μm, as illustrated in Fig. 6(c). We obtained the peak-to-peak amplitude of the microstructure as a function of the number of self-mixed signal stripes. The experimental results show that the number of signal fringes measured at different amplitudes corresponds to the peak amplitude of the object under test, following the basis of self-mixing theory.

In accordance with the limitation of the proposed technique, the resolution of SMI measurement used in this study is consistent with the conventional interferometry, which is $\lambda/2$ and the amplitude of the measured object should be greater than $\lambda/2$. The maximum vibration range of the measured object should be within the range of the transmitted light-gathering spot length. Otherwise, the measured object cannot be detected. As observed in the numerical simulation and calculation of the aqueous solution environment, the transmitted light aggregation spot length is approximately 6 μm. In our experimental environment, we control the amplitude of the measured object to gradually increase from $\lambda/2$ to explore the actual maximum measurement range. When the maximum vibration is set to 5.8 μm, the SMI phenomenon disappears.

The displacement of the measured signal was reconstructed by multiple Hilbert transform, and the experimental error is deduced. Five groups of experiments were performed, and the PZT was controlled as sinusoidal vibration with a frequency of 5 Hz and amplitudes of 1, 2, 3, 4, and 5 Hz to verify the measurement accuracy of this technique. Five experiments were conducted in each group, as shown in Table 1.

The SMI effect can only be observed when the probe light reaches the surface of the object under test and then returns to the laser cavity with motion information. In our experiment, if the fiber probe and the microstructure are not aligned to the same plane, then no self-mixing signal is generated. When the

fiber probe is not to the surface of the microstructure or is affected by Brownian motion in the specimen cavity, the self-mixing signal is disturbed and becomes unstable.

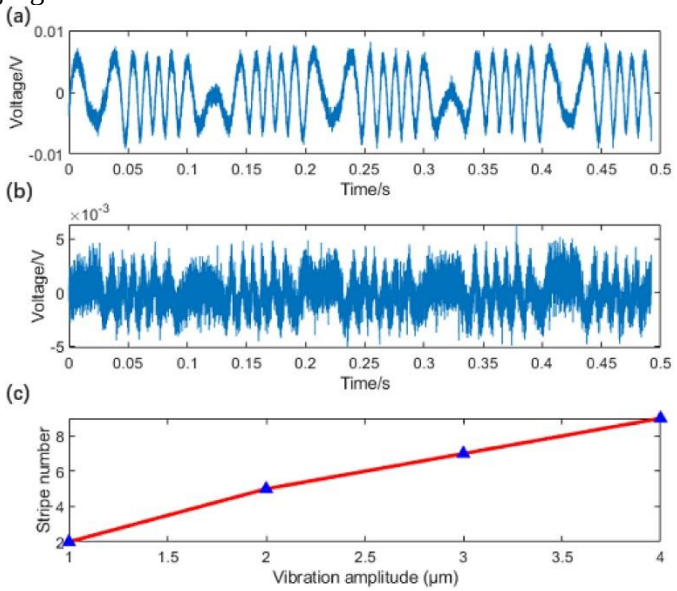

Fig. 6. (a) The self-mixing signal waveform is obtained using the fiber probe with BMS at a frequency of 5 Hz and amplitude of 3 μm respectively. (b) The self-mixing signal waveform is obtained using the fiber probe without BMS under the same conditions. (c) The relation between the peak-to-peak amplitude of the microstructure and the fringe number of the self-mixing signal which amplitude from 1.0 μm to 4.0 μm.

Table 1
Error analysis of actual and measured displacement.

Amplitude (μm)	Error (nm)
1	136
2	134
3	138
4	142
5	148

5. Discussion

Yeast cell culture: Yeast (Saccharomyces cerevisiae) was cultured in a lysogenic medium at room temperature for 48 h with a pH of 4.5 at 28 °C. It is selected during the early growth stage before bacterial spore formation because yeast cells have a regular shape at this stage. The yeast cells are then washed and diluted with phosphate-buffered saline to obtain the appropriate concentration. A trypan blue reagent (concentration: 0.5%, Solarbio) is added into the cell solution with a volume ratio of 1:9 to test the viability of the biomicrolens after laser irradiations. The result shows that the bio-microlens are not stained blue because the cells remained alive after our experiments. To better evaluate this work, we discussed it here on the basis of the limitations of lens cells and proposed some possible solutions. When compared with dielectric microspheres with a full uniform index of refraction, the cell's internal heterogeneous structure leads to a certain degree of interference due to the uneven refractive index to prevent the perfect light focusing. However, most of the material within the cell to near-infrared light are optically transparent. Thus, the absorption and scattering light optical relatively weak interactions occur inside a single cell. For bacterial cells, the cells within the refractive index are relatively uniform because they lack the nucleus and organelles. The shape of the cells can have the light of the relatively high optical power to adjust due to the inherent elastic membrane. This effect can be avoided by using medium-light power, such as the use of 30 mW power in our measuring experiments. From another perspective, the change in cell shape can facilitate the assembling of tunablelens, which is based on the unique properties of lens cells and cannot be achieved by the inorganic microsphere lenses. Certain

specific types of activities within the cell affect the capturing and focusing performance. For example, the movement of organelles and the cell activity of endocytosis change the refractive index distribution in the cell, causing optical distortion during the capture and measuring process. However, this effect is unremarkable because most organelles and endocytosis are relatively small compared with the wavelength of light. Some other cellular activities, such as cellular respiration, protein transport or DNA replication, are ultrafast processes that cannot be observed under an optical microscope; therefore, these activities have no effect on the capture and focus scheme.

The shape of some cells is round in exploring the real microorganisms in the future. Compared with our simulated surface with flat end microstructures, the measurement difficulty increases because the surface of the measured object is at a nonflat end, and the probe light needs to find a suitable measuring point to measure its displacement information. Unlike mechanical vibration, the vibration of biological cells is subject to unknown environmental fluctuations, and some potential challenges are still found in future applications.

6. Conclusion

In summary, microscale vibration detected by a living biological probe was previously undescribed. In this work, we suggested that the use of living yeast cells as microlens can greatly enhance the sensitivity and detection limit of optical fiber sensors in detecting microscale vibration. The developed system provides accurate and noninvasive cell manipulation, leading to a biocompatible approach in studying a wide range of microbiological measurements.

Declaration of Competing Interest

The authors declare that they have no known competing financial interests or personal relationships that could have appeared to influence the work reported in this paper.

Funding

Talent Project Fund of Heilongjiang Provincial Leading Talents Echelon, China [grant number No. 719900037]

References

[1] Bs C., Belloeil V., Plantier G., Gourinat Y., Bosch T., A self-mixing laser sensor design with an extended Kalman filter for optimal online structural analysis and damping evaluation, IEEE/ASME Trans. Mechatronics, 12 (2007), pp. 387-394

[2] Chen M., Zhang Y., Chen C., Wang L., Huang W., Damping microvibration measurement using laser diode self-mixing interference, IEEE Photon. J., 6 (2017), pp. 1-8

[3] Mehta A., Mohammed W., Johnson E.G., Multimode interference-based fiber-optic displacement sensor, IEEE Photonics Technol. Lett., 15 (2003), pp. 1129-1131

[4] Xu Z., Li J., Zhang S., Tan Y., Zhuang S., Remote eavesdropping at 200 meters distance based on laser feedback interferometry with single-photon sensitivity, Opt. Lasers Eng., 141 (2021), Article 106562

[5] Atashkhooei R., Urresty J.C., Royo S., Riba J.R., Runout tracking in electric motors using self-mixing interferometry, mechatronics, IEEE/ASME Trans., 19 (2014), pp. 184-190

[6] Bingkun G., Chen Q., Shunxin Y., Chen P., Chunlei J., Measurement of rotation speed based on double-beam self-mixing speckle interference, Opt. Lett., 43 (2018), p. 1531

[7] Alexandrova A.S., Tzoganis V., Welsch C.P., Laser diode self-mixing interferometry for velocity measurements, Opt. Eng., 54 (2015), Article 034104

[8] Donati S., Norgia M., Self-mixing interferometry for biomedical signals sensing, Sel. Top. Quantum Electron., 20 (2014), p. 6900108

[9] Julien P., Adam Q., Reza A., Francisco A., Evelio R.M., Olivier B., Ajit J., Antonio L.A., Carlos Y., Jesus C., Current developments on optical feedback interferometry as an all-optical sensor for biomedical applications, Sensors, 16 (2016), p. 694

[10] Arasanz A., Azcona F.J., Royo S., Jha A., Pladellorens J., A new method for the acquisition of arterial pulse wave using self-mixing interferometry, Opt. Laser Technol., 63 (2014), pp. 98-104

[11] Milesi I., Norgia M., Pompilio P.P., Svelto C., Dellaca R.L., Measurement of local chest wall displacement by a custom self-mixing laser interferometer, IEEE Trans. Instrum. Meas., 60 (2011), pp. 2894-2901
[12] Taimre T., Nikoli M., Bertling K., Lim Y.L., Raki A.D., Laser feedback interferometry: A tutorial on the self-mixing effect for coherent sensing, Adv. Optics Photonics, 7 (2015), p. 570
[13] Kasas S., Ruggeri F.S., Benadiba C., Maillard C., Stupar P., Tournu H., Dietler G., Longo G. Detecting nanoscale vibrations as signature of life, Proc. Natl. Acad. Sci. (2014), p. 112
[14] Pelling A.E., Sehati S., Gralla E.B., Valentine J.S., Gimzewski J.K., Local nanomechanical motion of the cell wall of saccharomyces cerevisiae, Science, 305 (2004), pp. 1147-1150
[15] Vo-Dinh T., Alarie J.P., Cullum B.M., Griffin G.D., Antibody-based nanoprobe for measurement of a fluorescent analyte in a single cell, Nature Biotechnol., 18 (2000), pp. 764-767
[16] Shambat G., Single-cell photonic nanocavity probes (presentation video), Reporters, Markers, Dyes, Nanoparticles, and Molecular Probes for Biomedical Applications VI (2014)
[17] Huang X., Jain P.K., El-Sayed I.H., El-Sayed M.A., Plasmonic photothermal therapy (PPTT) using gold nanoparticles, Lasers Med., 23 (2008), pp. 217-228
[18] Wang K., Schonbrun E., Steinvurzel P., Crozier K.B., Trapping and rotating nanoparticles using a plasmonic nano-tweezer with an integrated heat sink, Nature Commun., 2 (2011), p. 469
[19] Li Y., Liu X., Li B., Single-cell biomagnifier for optical nanoscopes and nanotweezers, Light: Sci. Appl., 8 (2019)
[20] Miccio L., Memmolo P., Merola F., Netti P.A., Ferraro P., Red blood cell as an adaptive optofluidic microlens, Nature Commun., 6 (2015), p. 6502
[21] Monks J.N., Bing Y., Hawkins N.A., Vollrath F., Wang Z., Spider silk: Mother nature's bio-superlens, Nano Lett., 16 (2016), p. 5842
[22] Hamid P., Mohammadreza K., Yao-Wei H., Zhujun S., Hariri L.P., Adams D.C., Vivien D., Alexander Z., Cheng-Wei Q., Federico C., Nano-optic endoscope for high-resolution optical coherence tomography in vivo, Nat. Photonics, 12 (2018)
[23] Rodriguez Sevilla P., Labrador-Páez L., Jaque Garcia D., Haro Gonzalez P., Optical trapping for biosensing: materials and applications, J. Mater. Chem. B (2017), 10.1039/C7TB01921A
[24] Svoboda K., Block S., Biological applications of optical forces, Annu. Rev. Biophys. Biomol. Struct., 23 (1994), pp. 247-285
[25] Kusumi A., Tsunoyama T.A., Hirosawa K.M., Kasai R., Fujiwara T., Tracking single molecules at work in living cells, Nat. Chem. Biol., 10 7 (2014), pp. 524-532
[26] Yong I.P., Kang T.L., Suh Y.D., Hyeon T., Upconverting nanoparticles: a versatile platform for wide-field two-photon microscopy and multi-modal in vivo imaging, Chem. Soc. Rev., 44 (2015)
[27] Zhang Z., Li C., Huang Z., Vibration measurement based on multiple Hilbert transform for self-mixing interferometry, Opt. Commun., 436 (2019), pp. 192-196
[28] Wang Y., Li Y., Xu X., Tian M., Tan Y., All-fiber laser feedback interferometry with 300m transmission distance, Opt. Lett. (2021)
[29] Zhao Y., Guo Y., Wang C., Yang B., Lu L., Design and experimental study of the biorthogonal linkage laser self-mixing angle sensor, Opt. Commun., 475 (2020), Article 126248
[30] Zhao Y.Y., Zhu D.S., Tu Y.R., Pi L.L., Li H.T., Xu L., Hu Z.J., Shen Y.C., Yu B.L., Lu L., Coherent laser detection of the femtowatt-level frequency-shifted optical feedback based on a DFB fiber laser, Opt. Lett., 46 (2021), pp. 1229-1232
[31] Chenchen W., Xuewei F., You G., Huaqiao G., Huanqing W., Jianguo L., Benli Y., Liang L., Full-circle range and microradian resolution angle measurement using the orthogonal mirror self-mixing interferometry, Opt. Express, 26 (2018) 10371
[32] Guo D., Quadrature demodulation technique for self-mixing interferometry displacement sensor Opt. Commun., 284 (2011), pp. 5766-5769